Nanoscale

Accepted Manuscript

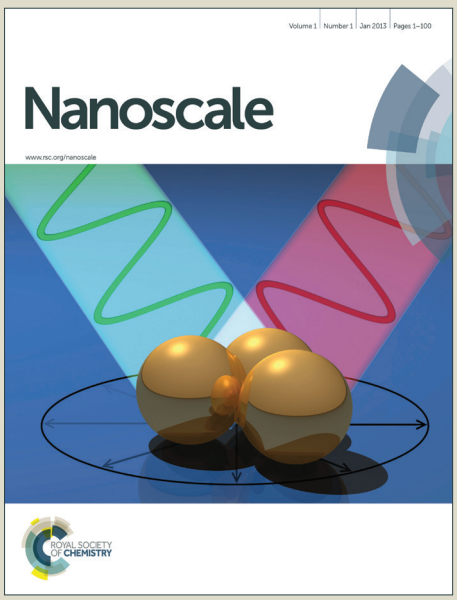

ROYAL SOCIETY OF CHEMISTRY

www.rsc.org/nanoscale

Journal Name

RSCPublishing

ARTICLE

A strategy to synergistically increase the number of active edge sites and the conductivity of MoS_2 nanosheets for hydrogen evolution†

Cite this: DOI: 10.1039/x0xx00000x

Received 00th January 2012,
Accepted 00th January 2012

DOI: 10.1039/x0xx00000x

www.rsc.org/

Hailong Yu,[a] Xianbo Yu,[a] Yujin Chen,*[a] Shen Zhang,[a] Peng Gao,*[b] and Chunyan Li*[a]

Due to more active edge sites, nanostructured MoS_2 as electrocatalyst is very promising for hydrogen evolution. However, a very large resistance between basal planes decreases its overall efficiency of hydrogen evolution, and great limits its application in industry. Herein we develop a facile strategy to synergistically increase the number of active edge sites and conductivity of MoS_2. By the facile strategy MoS_2 nanosheet arrays can be grown vertically on carbon fiber cloth (CFC) substrates. On one hand, ammonium fluoride in the reaction system could effectively etch the inert basal plane of MoS_2 nanosheets, leading to pits formed in the inert basal plane of MoS_2 nanosheets, and thereby the number of active edge sites is significantly increased. On the other hand, vertical growth of MoS_2 nanosheet arrays on CFC can significantly decrease the resistance of MoS_2-based electrocatalysts. As result, the MoS_2-based electrocatalysts exhibit excellent catalytic activity for hydrogen evolution reaction with a small Tafel slope and a large cathodic current density. Moreover, the CFC can be repeatedly utilized as a template to grow ultrathin MoS_2 nanosheet arrays for HER. The excellent activity and recyclable utilization as well as mass production indicate that the composite has promising application in industry.

1 Introduction

Hydrogen generation through electrolysis of water has been considered as a promising approach to replace traditional fossil fuels to solve the increasing energy crisis and environmental pollution.[1-3] Noble metals such as Pt are common used as hydrogen evolution reaction (HER) catalysts, which shows excellent performance and stability.[4, 5] However, the high cost and rare reserves of the noble metals limit in their industrial application. Recently, two-dimensional (2D) layered metal chalcogenide materials, such as MoS_2,[6-19] $MoSe_2$,[15, 18] WS_2[16, 20] and WSe_2, [18] exhibited high HER performances as they are used as electrocatalysts. Among those materials, MoS_2 has drawn great attention due to its low cost, high chemical stability, excellent electrocatalytic properties. [21]

MoS_2 naturally occurs as a lamellar hexagonally structure similar to that of graphite in which the individual S−Mo−S layers weakly interact with each other by van der Waals forces, and the distance between two neighboring layers can be expanded.[1, 7] Recently, both experimental and computational studies demonstrated that the electrocatalytic HER performance of MoS_2 were strongly dependent on the number of the active edge sites.[3, 6, 11, 17, 19] Therefore, if the size of MoS_2 decreases to the nanoscale, its active edge sites will significantly increase, leading to the improvement of its HER performance. For example, Xie and Lou's group have successful synthesized defect-rich MoS_2 ultrathin nanosheets.[17] The defect-rich MoS_2 ultrathin nanosheets displayed the large cathodic current density of 13 mA cm^{-2} at an overpotential of 200 mV. Besides the number of the active edge sites, the electrical transport of MoS_2 nanostructure plays an important role in HER performance. However, the extremely low conductivity between two adjacent van der Waals bonded S–Mo–S sheets significantly decreases the overall HER rate.[19] When semiconductive 2H-MoS_2 converts into metallic 1T-MoS_2, the HERs catalytic performance will be great improved due to low resistance of the 1T-MoS_2.[12, 21-23] Unfortunately, the 1T-MoS_2 is not stable, and its synthetic process is relatively complicated.[12, 21, 22] The resistance of 2H-MoS_2 electrodes can be also reduced to some degree when 2H-MoS_2 grows on conductive substrates such as carbon fiber paper and F-doped tin oxide glass (FTO) by the chemical vapor deposition method.[9, 16, 21] Nevertheless, synergistically structural and electronic modulations to increase the number of active edge sites and conductivity of MoS_2 simultaneously still remain challenging.[19]

In this work, we increase both the number of active edge sites and conductivity of MoS_2 simultaneously by a facile one-step hydrothermal method. MoS_2 nanosheet arrays can be

grown vertically on carbon fiber cloth (CFC) substrates (for convenience, the sample is named as CMSNA) by the facile strategy. On one hand, ammonium fluoride in the reaction system could effectively etch the inert basal plane of MoS_2 nanosheets, leading to pits formed in the basal plane of MoS_2 nanosheets, and thereby the numbers of active edge sites were significantly increased, as shown in Scheme 1(a). On the other hand, vertical growth of MoS_2 nanosheet arrays on CFC can significantly decrease the resistance of the composite. One of important reasons for poor HER performance of bulk MoS_2 is that the conductivity between two adjacent van der Waals bonded S–Mo–S sheets is extremely low. [24, 25] Resistivity through the basal planes was measured to be 2200 times larger than that through the direction parallel to the planes, which significantly decreases the overall HER rate. [26] If MoS_2 laid on the other types of conductive supports, the electrons have to be transferred from the support to the bottom layer and then further through layer interfaces to reach all the active sites, [24] as shown in the left part of Scheme 2(b). When the MoS_2 nanosheets are grown vertically on the CFC, the electrons can be transferred from highly conductive CFC directly to active edge sites of each single layer of MoS_2 nanosheets, as shown in the right part of Scheme 2(b). Such change in electron transfer path will significantly improve the conductivity of the resistance of the MoS_2 nanosheets for HER.[22] Besides, there are other additional advantages of our designed electrocatalysts including: (i) Any binders such as Nafion solution need not be used in the preparation process of the MoS_2-based electrodes, (ii) The network structure of the electrodes is in favor of the permeation of electrolyte and the escape of the hydrogen bubbles produced during HER process, and (iii) Importantly, the CFC is recyclable.

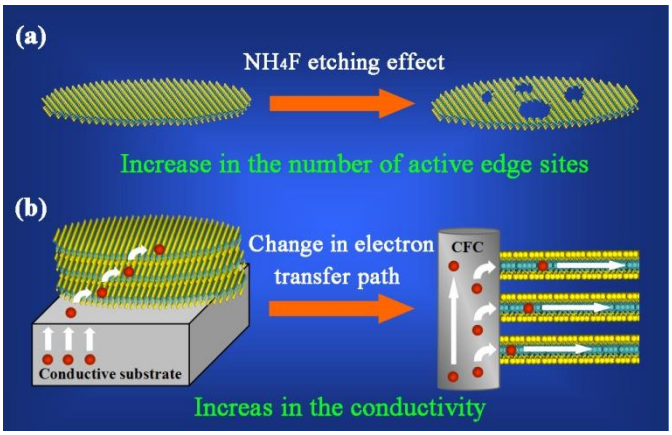

Scheme 1 illustration of synergistic increase in the number of active edge sites (a-b) and the conductivity of MoS_2 (c-d).

2 Experimental Section

2.1 Materials

Carbon fiber cloth was purchased from Cetech Co. Ltd. (Taiwan, China), and its through plate resistance is low than 5 mΩ cm^{-2}. All other reagents were analytically pure, and used without further purification.

2.2 Synthesis of CMSNA

The CMSNA was fabricated by a facile hydrothermal method. Typically, 30 mg of MoO_3, 45 mg of thioacetamide, and 300 mg of ammonium fluoride (NH_4F) were added to 30 mL distilled water under vigorous stirring for 30 min. Carbon fiber cloth (area: 5 cm^2) was immersed the mixture above under ultrasonication for 5 min. Then the mixture was transferred into a Teflon-lined stainless steel autoclave with a capacity of 40 mL for hydrothermal treatment at a 220°C temperature for 4, 8, and 12 h, respectively. The autoclave was cooled down to room temperature naturally, and then the CMSNAs were washed in distilled water and absolute ethanol under ultrasonication for 10 min, respectively, and dried in a vacuum oven at 60°C. The corresponding samples are named as CMSNA-4, CMSNA-8, and CMSNA-12, respectively.

For comparison, a sample was also prepared by replacing ammonium fluoride with urea.[27] Simply, 30 mg of MoO_3, and 486 mg of urea (the same molar quantity as that of ammonium fluoride), were added to 30 mL ethanol-water mixture under vigorous stirring for 30 min. Carbon fiber cloth (area: 5 cm^2) was immersed the mixture above under ultrasonication for 5 min. Then the mixture was transferred into a Teflon-lined stainless steel autoclave with a capacity of 40 mL for hydrothermal treatment at a 220°C for 8 h. The autoclave was cooled down to room temperature naturally, and then the sample was washed in distilled water and absolute ethanol under ultrasonication for 10 min, respectively, and dried in a vacuum oven at 60°C. The sample is named as CMSNA-U.

2.3 Characterization

The morphology and size of the synthesized CMSNAs were characterized by scanning electron microscope [HSD/SU70], an FEI Tecnai-F20 transmission electron microscope equipped with a Gatan imaging filter (GIF), and atomic force microscope (AFM, Veeco Dimension 3100). The crystal structure of the sample was determined by X-ray diffraction (XRD) [D/max 2550 V, Cu Ka radiation]. XPS measurements were carried out using a spectrometer with Al Kα radiation (PHI 5700 ESCA System). The binding energy was calibrated with the C 1s position of contaminant carbon in the vacuum chamber of the XPS instrument (284.6 eV).

2.4 Electrochemical Measurements

Electrochemical measurements were performed in a three-electrode system at an electrochemical station (CHI660D). The three-electrode configuration using an Ag/AgCl (KCl saturated) electrode as the reference electrode, a graphite rod as the counter electrode, and CMSNAs as the working electrode was adopted for polarization and electrolysis measurements. In addition, CMSNAs as the working electrode does not need any further treatment. Linear sweep voltammetry with scan rate of 3 mV s^{-1} was conducted in 0.5 M H_2SO_4 (purged with pure N_2). For a Tafel plot, the linear portion is fit to the Tafel equation.

All data have been corrected for a small ohmic drop based on impedance spectroscopy. All the potentials were calibrated to a reversible hydrogen electrode (RHE).

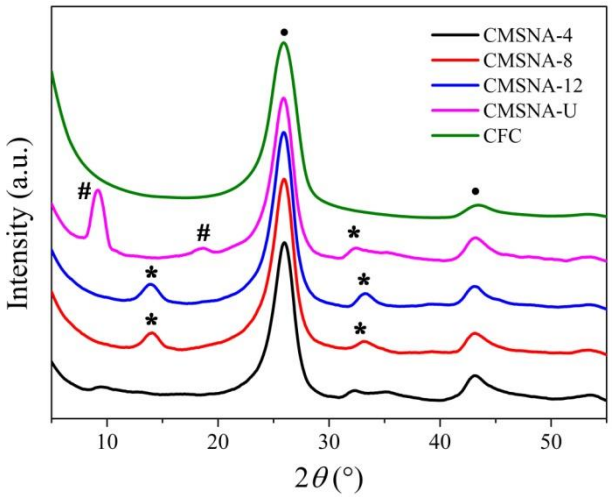

Figure 1 XRD patterns of CFC, CMSNA-4, CMSNA-8, CMSNA-12, and CMSNA-U.

3 Results and discussion

Figure 1 shows XRD patterns of CFC, CMSNA-4, CMSNA-8, CMSNA-12, and CMSNA-U, in which the diffraction peaks located at 2θ = 26.2 and 43.4°come from CFC. It can be found that the reaction time and type of reagents have important effect on the crystalline structure of MoS_2. As for the CMSNAs obtained with NH_4F in the reaction system, a short time will lead to a very poor crystallinity of MoS_2 in the sample such as CMSNA-4. As the reaction time is prolonged to above 8 h, the crystallinity of MoS_2 in the samples, such as CMSNA-8 and CMSNA-12, will be improved significantly. The diffraction peaks located at 2θ =14.0 and 33.0°, marked by "*", corresponds to the (002) and (100) crystal planes of 2H-MoS_2 (JCPDS No. 75–1539). However, as NH_4F is replaced with urea, besides the peak at 2θ =33.0°, two other peaks at 9.2 and 18.5°, marked by "#", are also observed in the pattern of CMSNA-U. Using the Bragg equation, the corresponding *d* spacings are 0.96 and 0.48 nm, respectively. This reveals that the interlayer distance of the (002) plane of MoS_2 is expanded.[28] The results above demonstrate that the crystal structure of MoS_2 can be tuned by the reaction time and types of reagent added in the reaction system.

The morphology and the structure of the final products were characterized by scanning electron microscopy (SEM) and transmission electron microscopy (TEM) analyses. Figure 2a_1-a_3, 2b_1-b_3, 2c_1-c_3, and 2d_1-d_3 are typical SEM images of CMSNA-4, CMSNA-8, CMSNA-12, and CMSNA-U with different magnifications, respectively. A similar ordered woven structure to the bare carbon cloth templates can be clearly observed in the low-magnification SEM images. The carbon fiber composite in CMSNA samples (Figure 2a_2, 2b_2, 2c_2) has a uniform diameter larger than that of bare carbon fiber (Fig.S1, see ESI).† From magnified SEM images (Fig. 2a_3, 2b_3, and 2c_3), it can be clearly seen that ultrathin MoS_2 nanosheets vertically grow uniformly on the surface of each carbon fiber. The lateral length and the thickness of individual MoS_2 nanosheets in CMSNA-U are the largest among the CMSNAs, and whereas the values in CMSNA-4, CMSNA-8, and CMSNA-12 are gradually decreased. The decrease in the lateral length and the thickness of individual MoS_2 nanosheets in CMSNA-4, CMSNA-8, and CMSNA-12 may be related to the NH_4F etching effect, as discussed latterly. It should be noted that there are MoS_2 spheres in CMSNA-12, which may suppress its HER activity.

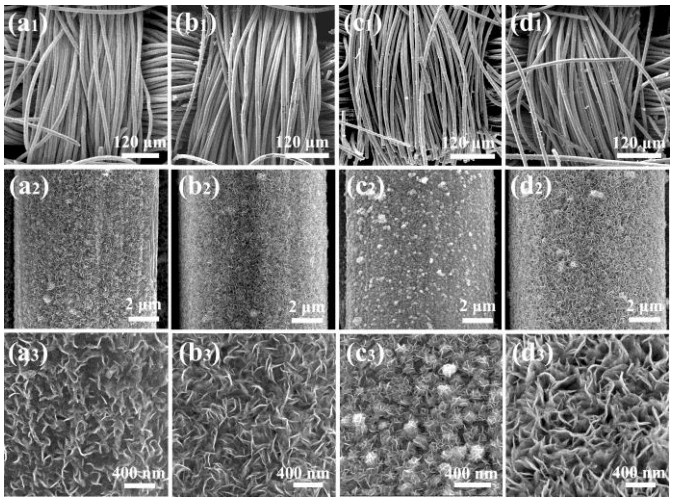

Figure 2 Typical SEM images of CMSNAs. (a_1-a_3) CMSNA-4, (b_1-b_3) CMSNA-8, (c_1-c_3) CMSNA-12, and (d_1-d_3) CMSNA-U.

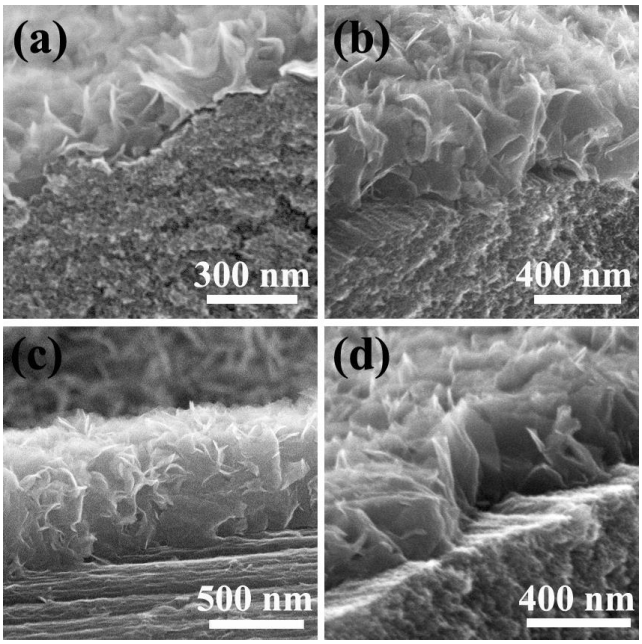

Figure 3 Cross-section SEM images of CMSNAs. (a) CMSNA-4, (b) CMSNA-8, (c) CMSNA-12, and (d) CMSNA-U.

The cross-section SEM images for CMSNAs are shown in Fig. 3. The measured height of the MoS_2 nanosheet arrays are

about 220, 480, 610, and 450 nm, respectively. This reveals that the loading density of the MoS_2 nanosheets in CMSNA-4, CMSNA-8, and CMSNA-12 are increased with the increase of the reaction time. The loading densities of the MoS_2 active materials in CMSNA-4, CMSNA-8, CMSNA-12, and CMSNA-U are calculated as 0.4, 1.6, 3.1, and 1.6 mg cm^{-2}, respectively.[27]

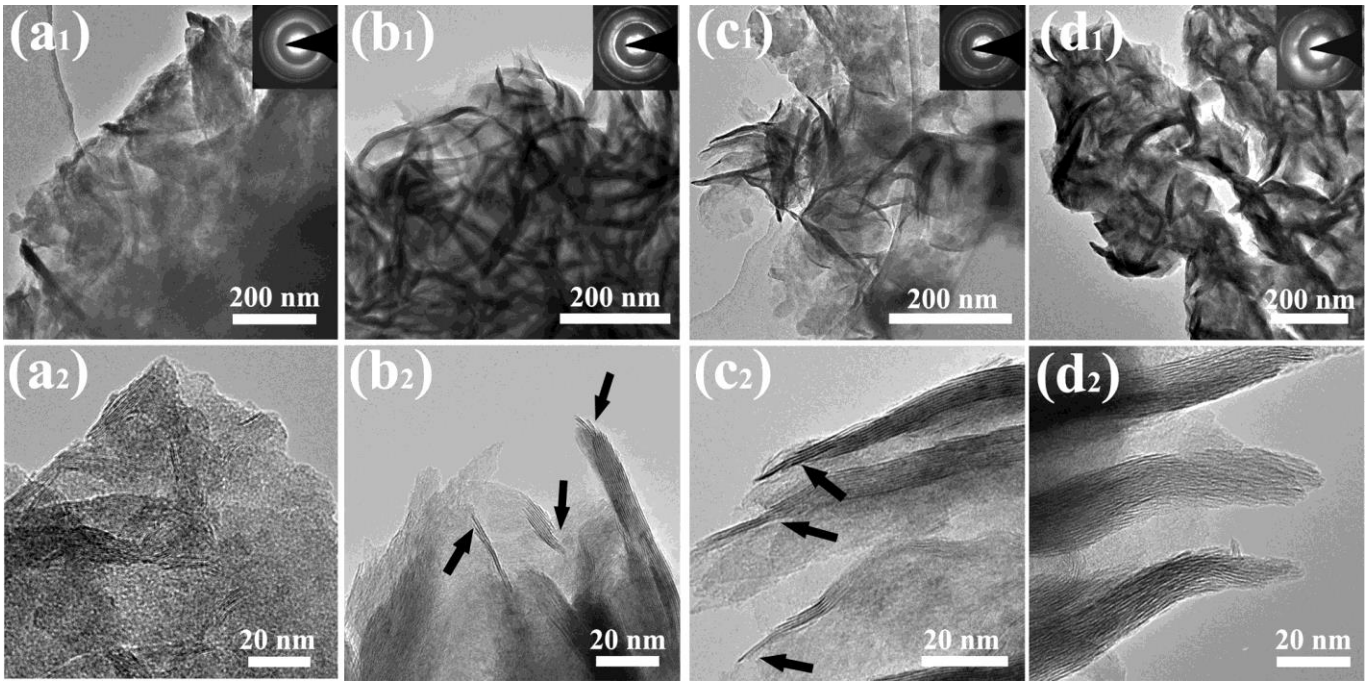

Figure 4 TEM images of MoS_2 nanosheets in CMSNAs. (a) CMSNA-4, (b) CMSNA-8, (c) CMSNA-12, and (d) CMSNA-U. The insets showing the corresponding SAED patterns of the MoS_2 nanosheets in CMSNAs.

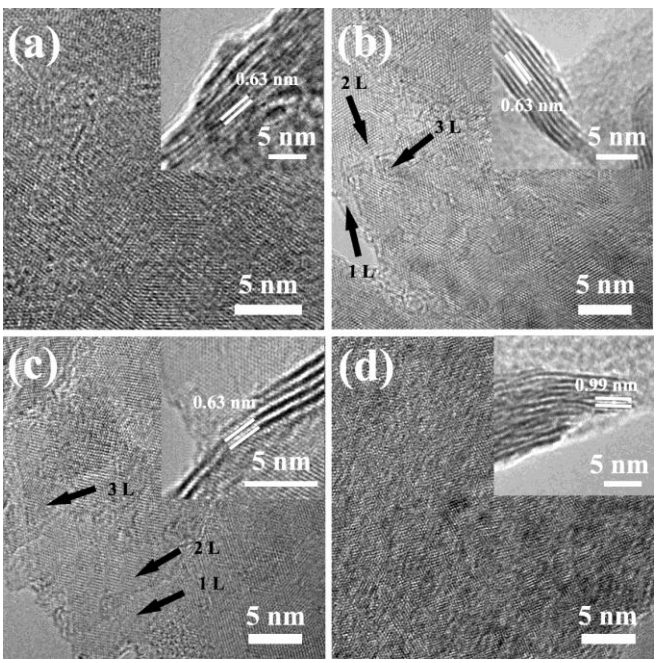

Figure 5 HRTEM images of basal planes of MoS_2 nanosheets in CMSNAs. (a) CMSNA-4, (b) CMSNA-8, (c) CMSNA-12, and (d) CMSNA-U.

Fig. 4 shows TEM images of the MoS_2 nanosheets in CMSNAs. The mean thicknesses of the MoS_2 nanosheets in CMSNA-4, CMSNA-8, CMSNA-12, and CMSNA-U are around 18, 9, 7, and 33 nm, respectively. The trend of the change in the thickness is consistent with SEM observations, which is related to the NH_4F etching effect. The crystallinity of MoS_2 in CMSNA-4, CMSNA-8, and CMSNA-12 is increased with the increase in the reaction time, as shown in the magnification TEM images and the selected-area electron diffraction patterns (SAED, the insets in low-magnification TEM images). The distances of (002) plane at the edges of the MoS_2 nanosheets in CMSNA-4, CMSNA-8, and CMSNA-12 are about 0.63 nm, whereas the value in CMSNA-U is about 0.99 nm, as shown in the insets of Fig. 5. It reveals that the presence of urea favors in expanding the distance of the (002) crystal plane of MoS_2, similar to the results previously reported.[17, 27, 28] The expanded interlayer distance of the (002) plane of MoS_2 in CMSNA-U was related to the synthesis conditions. The (002) plane are usually enlarged at the low temperature under the alkaline condition.[19, 27] It can be ascribed to oxygen incorporated into MoS_2 during the synthesis process.[19]

Interestingly, compared to MoS_2 nanosheets in CMSNA-4 and CMSNA-U, the ones in CMSNA-8 and CMSNA-12 have much thinner edges. As shown in Fig. 4 (b_2) and (c_2), the obvious stair-like edges between different layers, marked by arrows, can be observed in the edges of MoS_2 nanosheets in CMSNA-8 and CMSNA-12. However, such edges are not obviously discerned in CMSNA-U. Thus the stair-like edges can be attributed to the NH_4F etching effect. Due to the short

reaction time, such edges are also not conspicuous in CMSNA-4. In order to provide an evidence for the NH_4F etching effect, we carried out additional experiments. The experimental conditions were the same as those of CMSNA preparation except that MoO_3 was replaced with bulk MoS_2 (the size in micrometer level, Fig. S2) and the reaction time was 12 h.† As shown in Fig. S3, MoS_2 nanosheets can be grown on the CFC only in the case that NH_4F is presented in the reaction system, which demonstrates that NH_4F can etch bulk MoS_2, and decrease its size down to nanometer level.† This indicates that the NH_4F etching effect mainly contributes to the stair-like edges between different layers of the MoS_2 nanosheets. It is also the reason why the lateral length and the thickness of the middle region of the MoS_2 nanosheets in CMSNA-8 and CMSNA-12 are smaller than those in CMSNA-4 and CMSNA-U.

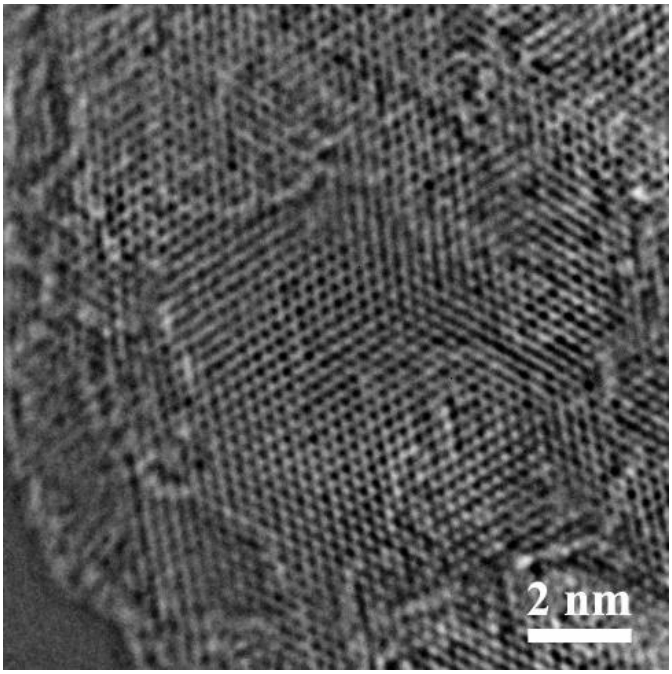

Figure 6 HRTEM images of typical basal plane of MoS_2 nanosheets in CMSNA-8.

In order to further investigate the NH_4F etching effect, the HRTEM analyses for the inert basal planes of the MoS_2 nanosheets in CMSNAs were carried out. As shown in Fig. 5, several single layers of MoS_2 (three single layers at least, marked by arrows) are emerged out in the basal plane of MoS_2 nanosheets in CMSNA-8 and CMSNA-12; however, they are not observed in CMSNA-4 and CMSNA-U. Furthermore, many pits are also formed in the inert basal plane of the MoS_2 nanosheets in CMSNA-8 and CMSNA-12 due to the NH_4F etching effect, as shown in Fig. 5(b) and (c). Such pits in CMSNA-8 can be more clearly observed in a magnification HRTEM image (Fig. 6) and the pits are marked in Fig. S4a). They are also presented in the AFM phase image (Fig. S4b) and c)).† The pits configurated in the inert basal plane of MoS_2 allow more active edge sites to expose to the electrolyte, and thereby the HER activity of the catalysts can be improved significantly.

The surface electronic state and composition of CMSNAs were analyzed by X-ray photoelectron spectroscopy (XPS) measurements. Fig. S5 show high-resolution Mo 3d spectra of CMSNAs.† Two peaks at 228.6 eV and 231.8 eV are observed in spectra, which correspond to the Mo^{4+} $3d_{5/2}$ and Mo^{4+} $3d_{3/2}$ components of MoS_2, respectively. † The $3d_{3/2}$ and $3d_{5/2}$ peaks have separation energies close to 3.1 eV, and the intensity ratio of the peaks is about 2: 3, characteristics of Mo species.[9, 24-27] The peak at around 225.7 eV corresponds to the S 2s component of MoS_2.[28, 29] The weak peaks at 223.0 eV and 236.0 eV correspond to Mo^{6+} species, indicating the oxidation of Mo_2S is minimal. In the high-resolution S 2p spectra (Fig. S6), the peaks at 161.4 eV and 162.7 eV are observed, corresponding to S^{2-} $2p_{3/2}$ and S^{2-} $2p_{1/2}$, respectively.†

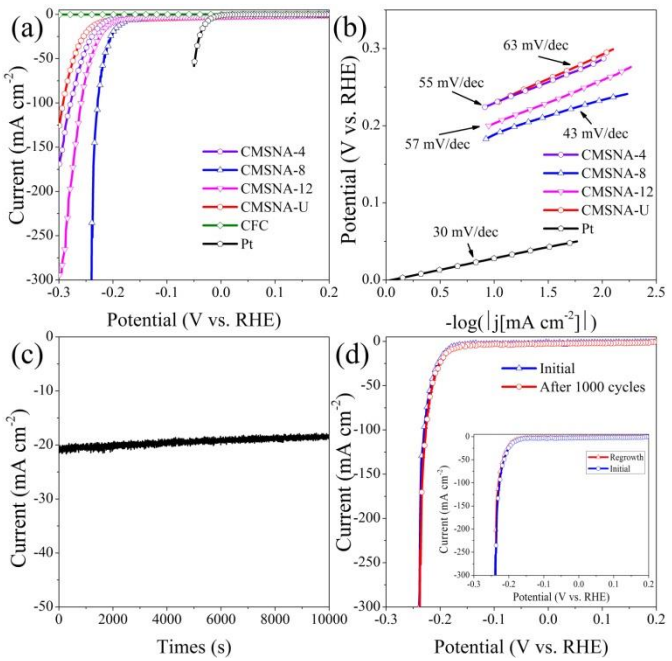

Figure 7 (a) Polarization curves of CMSNAs, Pt, and CFC, (b) Tafel plots of CMSNAs, and Pt, (c) Cycling stability of CMSNA-8 at an overpotential of 200 mV, (d) the polarization curvsw before and after potential sweeps for 1000 cycles in 0.5 M H_2SO_4 solution. The inset showing the comparison of the polarization curves between the MoS_2 nanosheet arrays grown (initial) and regrown on the CFC.

Electrochemical measurements of various CMSNA samples as well as the CFC and Pt were directly performed without any binders in 0.5 M H_2SO_4 solution using a three-electrode setup to investigate their HER activities. Fig. 7(a) shows the polarization curves with a sweep rate of 3 mV s^{-1}. Pt catalyst exhibits expected HER activity with a near zero overpotential (η), whereas the CFC exhibits negligible HER activity. In contrast, all the CMSNAs exhibit a relatively high HER activity. Among CMSNA samples, CMSNA-8 exhibits an onset overpotential (η) of 121 mV, smaller than those of CMSNA-4 (137 mV), CMSNA-12 (132 mV), and CMSNA-U (167 mV). Furthermore, the cathodic current rises rapidly at more negative

potentials for all the CMSANs. Notably, CMSNA-8 exhibits an extremely large cathodic current density of 365 mA cm^{-2} at η= 250 mV, great larger than that of bare carbon fiber cloth, and about 8.8, 4.9, and 1.33 times larger than those of CMSNA-4, CMSNA-12, and CMSNA-U. This current density is also larger than those of other nanostructured MoS_2 and MoS_2-based composites (Tab. 1), [11, 14, 17, 19, 30] which further indicates superior catalytic activity of CMSNA-8 for HER. The large current density means prominent hydrogen evolution behavior, evidenced by the continuous and small bubbles escaped from the CMSNA-8 electrode surfaces (video, ESI).†

Table 1 Comparisons of HER performances among different MoS_2-based atalysts

Catalyst type	Tafel slope	j_{250}	Refs
Double-gyroid MoS_2	50	11	11
Oxygen-Incorporated MoS_2	55	60	19
Rich-defect MoS_2	50	40	17
MoS_2/RGO	41	–	8
MoSx/3D Graphene	43	90	14
1T-MoS_2/carbon paper	43	200	12
1T-MoS_2	45	40	23
Exfoliated MoS_2	74	9	30
CMS-H	67	25	this work
CMSNA-4	55	39	this work
CMSNA-8	43	365	this work
CMSNA-12	57	71	this work
CMSNA-U	63	22	this work

Units for Tafel slope and j_{250} are mV dec^{-1} and mA cm^{-2}, respectively, and the j_{250} denotes the current density at η=250 mV.

For further study of HER activity of the CMSNAs, Tafel plots were fitted to Tafel equation ($\eta = a + b\log|j|$), where b is the Tafel slope. As shown in Fig. 7(b), the Pt catalyst exhibits a Tafel slope of 30 mV dec^{-1}, which is consistent with the reported values. The Tafel slope of CMSNA-8 (43 mV dec^{-1}) is the smallest among the CMSNAs. Furthermore, the value is only slightly larger than that of MoS_2/RGO (41 mV dec^{-1}), as shown in Tab. 1. Thus, CMSNA-8 exhibits excellent HER activity, which is attributed to both the increase in the number of active edge sites and the conductivity of MoS_2. As shown in TEM images (Fig. 5), the basal planes of MoS_2 nanosheets in CMSNA-8 and CMSNA-12 are etched to form many pits, which may lead to the increase of the numbers of active sites. In order to visualize the increase, the numbers of active sites of CMSNA samples were estimated in phosphate buffer solution (PH=7.0) according to a method previously reported.[13] As shown in Table S1, the numbers of the active sites of CMSNA-8 (2.6×10^{-7} mol cm^{-2}) and CMSNA-12 (3.0×10^{-7} mol cm^{-2}) are higher than those of CMSNA-4 (1.7×10^{-7} mol cm^{-2}) and CMSNA-U (1.1×10^{-7} mol cm^{-2}). Due to larger height of MoS_2 nanosheet arrays in CMSNA-12 (Fig. 3), parts of MoS_2 active materials are not contact with electrolyte effectively, which will suppress catalytic performance of CMSNA-12. On the other hand, the charge transfer resistance (R_{ct}) also play a very important role in HER activity of MoS_2 catalysts. Higher R_{ct} value would lead to very poor HER activity of MoS_2 catalysts.[17–19] In order to extract the resistance, electrochemical impedance spectroscopy (EIS) measurements were conducted. Fig. S7 shows the measured Nyquist plots of CMSNAs at 250 mV.† The data were fitted to equivalent circuit shown in the inset in Fig. S7.† According to the data and the equivalent circuit, the charge transfer resistance of CMSNA-8 is 1.6 Ω cm^{-2}, which is lower than those of CMSNA-4 (4.5 Ω cm^{-2}), CMSNA-12 (3.6 Ω cm^{-2}), and (5.8 Ω cm^{-2}). Thus the superior activity of CMSNA-8 for HER is also ascribed to its high conductivity. In order to futher provide an additional direct evidence that the MoS_2 nanosheet arrays vertically grown on CFC benefits the improvement of the conductivity, we grow MoS_2 nanosheets horizontally on CFC by the method previously reported (see the synthesis process in ESI).[31]† For convenience, the sample is named as CMS-H. SEM image (Fig. S8) shows that the MoS_2 nanosheets with a size of about 250 nm are horizontally grown on CFC.† XPS measurements (Fig. S9) are consistent with the previous results,[31] confirming the formation of MoS_2 on the CFC.† The HER activity of CMS-H was evulated under the same electrochemical conditons as those of the CMSNA samples. As shown in Fig. S10(a), CMS-H exhibits a cathodic current density of 25 mA cm^{-2} at η= 250 mV, great lower than those of CMSNA-4, CMSNA-8, and CMSNA-12 (also shown inTable 1).† Furthermore, the Tafel slope of CMS-H is 67 mV dec^{-1}, which is larger than those of CMSNA-4, CMSNA-8, and CMSNA-12 (Fig. S10(b) and Table 1).† The results above reveal that CMSNA samples exhibit superior HER activity to CMS-H. As illustrated in Scheme 1, CMSNAs exhibiting superior HER activities to CMS-H can be attributed to their higher conductivities, which is proved by the Nyquist plots of CMSNAs and CMS-H (Fig. S11) at various overpotentials.† In terms of the data and the equivalent circuit (the inset of Fig. S7), R_{ct} values of these samples can be determined and listed in Table 2. As expected, the R_{ct} values of CMS-H are larger than those of CMSNA samples at all the measured overpotentials. This demonstrates that vertical growth of MoS_2 nanosheet arrays on CFC as HER catalysts is more advantageous to horizontal growth of MoS_2 on CFC. CMSNA-8 has the lowest R_{ct} values among the samples, leading to its superior HER activity.

Table 2 Comparison of R_{ct} values of the different samples at different overpotentials

Materials	R_{ct} (Ω cm^{-2}) at η =250 mV	R_{ct} (Ω cm^{-2}) at η =200 mV	R_{ct} (Ω cm^{-2}) at η =150 mV	R_{ct} (Ω cm^{-2}) at η =100 mV
CMSNA-4	4.5	13.2	138.3	596
CMSNA-8	1.6	7.7	28.8	124
CMSNA-12	3.6	9.8	31.7	154
CMSNA-U	5.8	29.2	183.1	1328
CMS-H	12.7	54.6	295.5	2037

To investigate the stability during HER process, a long-term cycling test and continuous HER at a given overpotential were carried out. As shown in Fig. 7c, as an overpotential of 200 mV was applied, CMSNA-8 exhibited a continuous HER behavior. After a period of 10 000 seconds, the cathodic current density has almost not any degradation. The stability of CMSNA-8 in

acidic media was also investigated by sweeping the catalysts for 1000 cycles. After the cycles, the negligible current loss is observed, as shown in Fig. 7(d). SEM image (Fig. S12) of the sample after the stability test at an overpotential of 200 mV shows that the MoS_2 nanosheets with little change in the morphology are still grown vertically on the carbon fiber cloth, also suggesting the excellent durability of the sample for HER catalysts.†

Furthermore, CMSNA as electrocatalyst for HER posses an additional advantage, i.e., the carbon fiber cloth in the sample can be used repeatedly. After a long-term test, the MoS_2 nanosheets on the carbon fiber cloth can dissolve into 20% hydrogen nitrate solution by a hydrothermal treatment at 150°C, as shown in Fig. S13.† The bare carbon fiber can be used as template to regrow MoS_2 nanosheet arrays on its surfaces, as shown in Fig. S14.† Importantly, the MoS_2 nanosheets regrown on the carbon fiber still exhibits excellent HER performance, as shown the inset in Fig. 7d.

4 Conclusions

In summary, we develop a facile hydrothermal method to grow ultrathin MoS_2 nanosheets vertically on the surfaces of carbon fiber cloth. Due to the NH_4F etching effect, the number of active edge sites of MoS_2 can be increased significantly. At the same time, the electrons can be transferred from highly conductive CFC directly to active edges of each single layer of MoS_2 nanosheets, and thereby the conductivity of MoS_2 can be increased considerably. The increase both in the number of active edge sites and the conductivity lead to superior activity of the MoS_2-based composite for HER. Furthermore, the carbon fiber cloth in the composite can be used repeatedly for HER. The composite with excellent HER activity and recyclable utilization as well as mass production is suitable for practical applications in industry. The strategy presented here may open a way to improve HER activities of other Mo-based catalysts.

Acknowledgements

We thank the National Natural Science Foundation of China (Grant Nos. 51272050 and 21271053), the Innovation Foundation of Harbin City (2012RFXXG096), and also the 111 project (B13015) of Ministry Education of China to the Harbin Engineering University.

Notes and references

[a] *Key Laboratory of In-Fiber Intregrated Optics, Ministry of Education, and College of Science, Harbin Engineering University, Harbin 150001, China. Fax: 86-451-82519754; Tel: 86-451-82519754; E-mail: chenyujin@hrbeu.edu.cn and chunyanli@hrbeu.edu.cn*

[b] *College of Materials Science and Chemical Engineering, Harbin Engineering University, Harbin, 150001, China. E-mail: gaopeng@hrbeu.edu.cn*

Electronic Supplementary Information (ESI) available: [SEM images of CFC, bulk MoS_2, samples obtained as bulk MoS_2 replaced with MoO_3 in the presence of NH_4F or urea in the reaction system, CMSNA-8 after a long-term stability test, CMSNA-8 after a long-term test and then treated in the HNO_3 solution at 150°C, regrown sample, XPS spectra for CMSNAs, Nyquist plots of impedance spectroscopy analysis.]. See DOI: 10.1039/b000000x/

1 T. E. Mallouk, *Nat. Chem.*, 2013, **5**, 362.
2 K. Zeng and D. K. Zhang, *Prog. Energ. Combust.*, 2010, **36**, 307.
3 H. I. Karunadasa, E. Montalvo, Y. Sun, M. Majda, J. R. Long and C. J. Chang, *Science*, 2012, **335**, 698.
4 J. K. Norskov and C. H. Christensen, *Science*, 2006, **312**, 1322.
5 J. Greeley, T. F. Jaramillo, J. Bonde, I. Chorkendorff and J. K. Norskov, *Nat. Mater.*, 2006, **5**, 909.
6 B. Hinnemann, P. G. Moses, J. Bonde, K. P. Jørgensen, J. H. Nielsen, S. Horch, I. Chorkendorff and J. K. Nørskov, *J. Am. Chem. Soc.*, 2005, **127**, 5308.
7 T. F. Jaramillo, K. P. Jørgensen, J. Bonde, J. H. Nielsen, S. Horch and I. Chorkendorff, *Science*, 2007, **317**, 100.
8 Y. G. Li, H. L. Wang, L. M. Xie, Y. Y. Liang, G. S. Hong and H. J. Dai, *J. Am. Chem. Soc.*, 2011, **133**, 7296.
9 Z. Chen, D. Cummins, B. N. Reinecke, E. Clark, M. K. Sunkara and T. F. Jaramillo, *Nano Lett.*, 2011, **11**, 4168.
10 D. Merki, H. Vrubel, L. Rovelli, S. Fierro and X. Hu, *Chem. Sci.*, 2012, **3**, 2515.
11 J. Kibsgaard, Z. Chen, B. N. Reinecke and T. F. Jaramillo, *Nat.Mater.*, 2012, **11**, 963.
12 M. A. Lukowski, A. S. Daniel, F. Meng, A. Forticaux, L. Li and S. Jin, *J. Am. Chem. Soc.*, 2013, **135**, 10274.
13 D. Merki, S. Fierro, H. Vrubel and X. Hu, *Chem. Sci.*, 2011, **2**,1262.
14 Y. H. Chang, C. T. Lin, T. Y. Chen, C. L. Hsu, Y. H. Lee, W. J. Zhang, K. H. Wei and L. J. Li, *Adv. Mater.*, 2013, **25**, 756.
15 D. Kong, H. Wang, J. J. Cha, M. Pasta, K. J. Koski, J. Yao and Y. Cui, *Nano Lett.*, 2013, **13**, 1341.
16 D. Merki and X. Hu, *Energy Environ. Sci.*, 2011, **4**, 3878.
17 J. F. Xie, H. Zhang, S. Li, R. X. Wang, X. Sun, M. Zhou, J. F. Zhou, X. W. Lou and Y. Xie, *Adv. Mater.*, 2013, **25**, 5807.
18 H. Wang, D. Kong, P. Johanes, J. J. Cha, G. Zheng, K. Yan, N. Liu and Y. Cui, *Nano Lett.*,2013, **13**, 3426.
19 J. F. Xie, J. J. Zhang, S. Li, F. Grote, X. D. Zhang, H. Zhang, R. X. Wang, Y. Lei, B. C. Pan and Y. Xie, *J. Am. Chem. Soc.*, 2013, **135**, 17881.
20 D. Voiry, H. Yamaguchi, J. Li, R. Silva, D. C. B. Alves, T. Fujita, M. Chen, T. Asefa, V. B. Shenoy, G. Eda and M. Chhowalla, *Nat.Mater.*, 2013, **12**, 850.
21 Y. Yan, B. Y. Xia, Z. C. Xu, and X. Wang, *ACS Catal.*, 2014, **4**, 1693.
22 H. T. Wang, Z. Y. Lu, D. S. Kong, J. Sun, T. M. Hymel and Y. Cui, *ACS Nano*, 2014, **5**, 4940.
23 D. Voiry, M. Salehi, R. Silva, T. Fujita, M. W. Chen, T. Asefa, V. B. Shenoy, G. Eda and M. Chhowalla, *Nano Lett.*, 2013, **13**, 6222.
24 H. Tributsch, *Berich. Bunsen Gesell*, 1977, **81**, 361.
25 A. B. Laursen, S. Kegnæs, S. Dahl and I. Chorkendorff, *Energy Environ. Sci.*, 2012, **5**, 5577.
26 T. A. Patterson, J. C. Carver, D. E. Leyden and D. M. Hercules, *J. Phys. Chem.*, 1976, **80**, 1700.
27 H. L. Yu, C.L. Zhu, K. Zhang, Y. J. Chen, C. Y. Li, P. Gao, P. P. Yang and Q. Y. Ouyang, *J. Mater. Chem. A.*, 2014, **2**, 4551.
28 K. Zhang, Y. Zhao, S. Zhang, H. Yu, Y. Chen, P. Gao, C. Zhu, *J. Mater. Chem. A*, 2014, **2**, 18715.
29 H. W. Wang, P. Skeldon and G. E. Thompson, *Surf. Coat. Technol.*, 1997, **91**, 200.
30 D. Gopalakrishnan, D. Damien, and M. M. Shaijumon, *ACS nano*, 2014, **8**, 5297.
31 Y. M. Shi, Y. Wang, J. I. Wong, A. Y. S. Tan, C. L. Hsu, L. J. Li, Y. C. Lu and H. Y. Yang, *scientific reports*, 2013, **3**, 2169.